LETTER

doi:10.1038/nature09594

Tension directly stabilizes reconstituted kinetochore–microtubule attachments

Bungo Akiyoshi[1,2]*, Krishna K. Sarangapani[3]*, Andrew F. Powers[3]*, Christian R. Nelson[1], Steve L. Reichow[4], Hugo Arellano-Santoyo[1,2,3], Tamir Gonen[4,5], Jeffrey A. Ranish[6], Charles L. Asbury[3] & Sue Biggins[1]

Kinetochores are macromolecular machines that couple chromosomes to dynamic microtubule tips during cell division, thereby generating force to segregate the chromosomes[1,2]. Accurate segregation depends on selective stabilization of correct 'bi-oriented' kinetochore–microtubule attachments, which come under tension as the result of opposing forces exerted by microtubules[3]. Tension is thought to stabilize these bi-oriented attachments indirectly, by suppressing the destabilizing activity of a kinase, Aurora B[4,5]. However, a complete mechanistic understanding of the role of tension requires reconstitution of kinetochore–microtubule attachments for biochemical and biophysical analyses *in vitro*. Here we show that native kinetochore particles retaining the majority of kinetochore proteins can be purified from budding yeast and used to reconstitute dynamic microtubule attachments. Individual kinetochore particles maintain load-bearing associations with assembling and disassembling ends of single microtubules for >30 min, providing a close match to the persistent coupling seen *in vivo* between budding yeast kinetochores and single microtubules[6]. Moreover, tension increases the lifetimes of the reconstituted attachments directly, through a catch bond-like mechanism that does not require Aurora B[7–10]. On the basis of these findings, we propose that tension selectively stabilizes proper kinetochore–microtubule attachments *in vivo* through a combination of direct mechanical stabilization and tension-dependent phosphoregulation.

To isolate native yeast kinetochores, we modified a method that we previously developed to purify minichromosomes containing centromere-bound kinetochores[11]. We affinity-purified the Dsn1–Flag epitope-tagged kinetochore protein under physiological concentrations of salt to maintain kinetochore structure[11]. Although Dsn1 is a component of the four-member Mis12 kinetochore subcomplex (also called Mtw1/MIND complex[12]), silver-staining (Fig. 1a) and immunoblotting (Fig. 1b) of the detergent-eluate after SDS–polyacrylamide gel electrophoresis (SDS–PAGE) revealed co-purification of components from nearly all core subcomplexes. In contrast, purifications via tags on subcomplexes other than Mis12 did not isolate the majority of kinetochore subcomplexes (Supplementary Fig. 1 and refs 12, 13).

Kinetochore components were the most abundant proteins in the Dsn1–Flag-purified sample. Most bands on the silver-stained gels could be unambiguously assigned to core kinetochore proteins by gel shifts after epitope tagging (Supplementary Fig. 2), and their relative abundance was consistent between preparations (Figs 1a, 2a and Supplementary Figs 2, 4 and 6). Similarly, mass spectrometry indicated that core kinetochore proteins were the most abundant (Fig. 1c, Supplementary Table 1 and Supplementary Note 1). Spindle checkpoint and other kinetochore regulatory proteins also co-purified, although motor proteins and the Aurora B protein kinase were not detected (Supplementary Table 1 and Supplementary Note 2). To test whether the kinetochore proteins stably associate with Dsn1–Flag, we performed gel filtration after Flag peptide elution. A peak fraction (~25 nm Stokes radius) containing DNA- and microtubule-binding kinetochore components was detected (Fig. 1d, Supplementary Fig. 3 and Supplementary Note 3). Taken together, these data show that stable, large assemblies spanning the entire kinetochore can be isolated from budding yeast.

To investigate whether the purified kinetochore particles are functional, we developed several bead- and fluorescence-based assays. First, we double-tagged Dsn1 so the particles could be coupled via anti-penta-His antibodies to polystyrene microbeads. Beads prepared with kinetochore particles from wild-type cells bound densely along taxol-stabilized microtubules (22 ± 1 beads per field; Fig. 2b). If instead the beads were prepared using particles from *ndc80-1* (*NDC80* is also known as *TID3*) or *spc105-15* mutant strains (Fig. 2a and Supplementary Fig. 4), binding was severely reduced (2 ± 1 or 4 ± 1 beads per field, respectively; Fig. 2b). Fluorescent kinetochore particles from strains containing the centromeric histone variant Cse4 fused to green fluorescent protein (Cse4–GFP) behaved similarly (Fig. 2c, Supplementary Figs 5 and 6). Previous work using recombinant Ndc80 and Spc105 has suggested that both subcomplexes contribute synergistically to microtubule binding[14]. The marked loss of binding in our assays with either *ndc80-1* or *spc105-15* is consistent with this hypothesis. Notably, kinetochore particles from *dad1-1* mutants (Dam1 complex) supported binding at near wild-type levels (18 ± 3 beads per field; Fig. 2b). This observation is consistent with previous analyses indicating that the initial attachment of kinetochores to the sides of microtubules does not require the Dam1 complex[15].

During mitosis *in vivo*, kinetochores persistently attach to the assembling and disassembling ends of microtubules, and they withstand tensile forces ranging from about 0.4 to 8.0 pN[3,16]. Time-lapse fluorescence imaging confirmed that the kinetochore particles track with disassembling ends *in vitro* (Fig. 2d, Supplementary Fig. 7, Supplementary Movies 1 and 2 and Supplementary Notes 4 and 5). Their disassembly-driven movement was highly processive, usually continuing until the filament depolymerized completely back to the seed. To test whether they also withstand physiological forces, we adapted a recently-developed bead motility assay[16–19]. Beads prepared with kinetochore particles from wild-type and various mutant strains were attached near the growing ends of individual microtubules and constant tension was applied using a servo-controlled laser trap. Bead-bound wild-type particles remained associated with the microtubule end, supporting continuous loads up to 11 pN (Fig. 3a, Supplementary Fig. 8 and Supplementary Notes 4 and 5). These wild-type attachments were long lived, with a mean duration comparable to that of mitosis in yeast (Supplementary Fig. 9)[6]. They often persisted through multiple 'catastrophe' and 'rescue' events, where the filament switched from assembly to disassembly and vice versa (Fig. 3a, red trace, Supplementary Fig. 8 and Supplementary Movie 3), a behaviour exhibited by

[1]Division of Basic Sciences, Fred Hutchinson Cancer Research Center, Seattle, Washington 98109, USA. [2]Molecular and Cellular Biology Program, University of Washington, Seattle, Washington 98195, USA. [3]Department of Physiology & Biophysics, University of Washington, Seattle, Washington 98195, USA. [4]Department of Biochemistry, University of Washington, Seattle, Washington 98195, USA. [5]Howard Hughes Medical Institute, University of Washington, Seattle, Washington 98195, USA. [6]Institute for Systems Biology, Seattle, Washington 98103, USA.
*These authors contributed equally to this work.

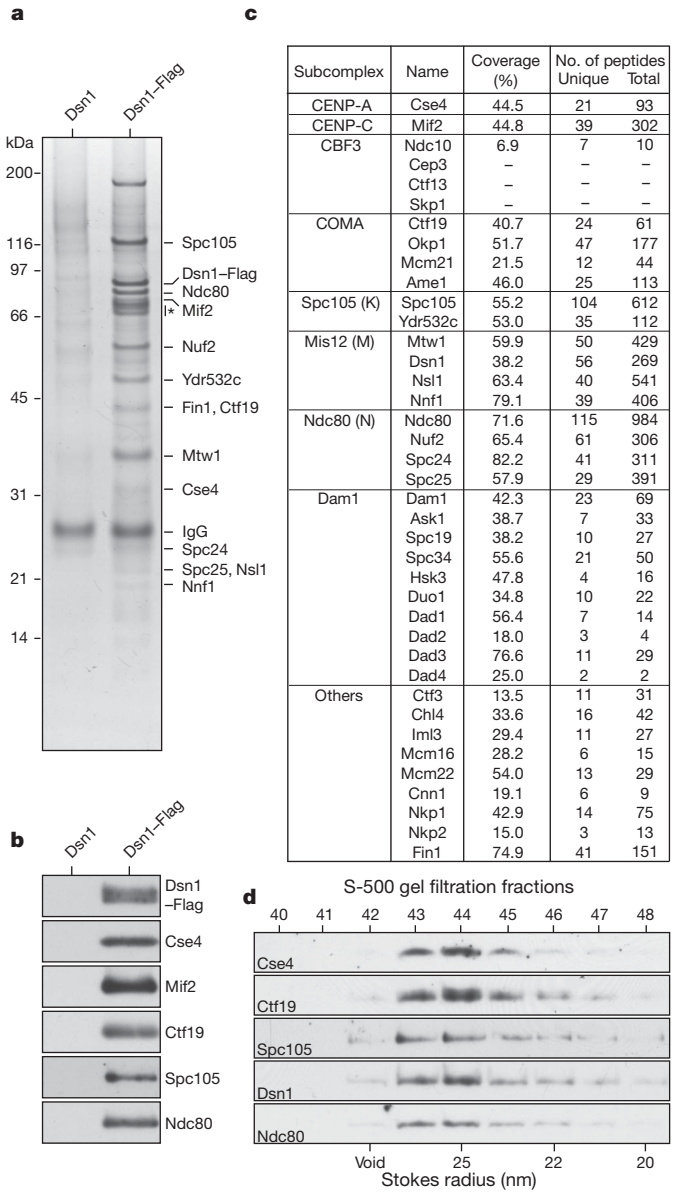

Subcomplex	Name	Coverage (%)	No. of peptides Unique	Total
CENP-A	Cse4	44.5	21	93
CENP-C	Mif2	44.8	39	302
CBF3	Ndc10	6.9	7	10
	Cep3	–	–	–
	Ctf13	–	–	–
	Skp1	–	–	–
COMA	Ctf19	40.7	24	61
	Okp1	51.7	47	177
	Mcm21	21.5	12	44
	Ame1	46.0	25	113
Spc105 (K)	Spc105	55.2	104	612
	Ydr532c	53.0	35	112
Mis12 (M)	Mtw1	59.9	50	429
	Dsn1	38.2	56	269
	Nsl1	63.4	40	541
	Nnf1	79.1	39	406
Ndc80 (N)	Ndc80	71.6	115	984
	Nuf2	65.4	61	306
	Spc24	82.2	41	311
	Spc25	57.9	29	391
Dam1	Dam1	42.3	23	69
	Ask1	38.7	7	33
	Spc19	38.2	10	27
	Spc34	55.6	21	50
	Hsk3	47.8	4	16
	Duo1	34.8	10	22
	Dad1	56.4	7	14
	Dad2	18.0	3	4
	Dad3	76.6	11	29
	Dad4	25.0	2	2
Others	Ctf3	13.5	11	31
	Chl4	33.6	16	42
	Iml3	29.4	11	27
	Mcm16	28.2	6	15
	Mcm22	54.0	13	29
	Cnn1	19.1	6	9
	Nkp1	42.9	14	75
	Nkp2	15.0	3	13
	Fin1	74.9	41	151

Figure 1 | Kinetochore particles can be isolated by affinity purification of Dsn1–Flag. **a**, Core kinetochore proteins co-purify with Dsn1–Flag as visualized by silver-stained SDS–PAGE. Asterisk indicates non-specific co-purifying proteins. **b**, Immunoblot confirms co-association of DNA- and microtubule-binding components with Dsn1–Flag. **c**, Mass spectrometry identifies all components of kinetochore subcomplexes except CBF3. Identities, percent sequence coverage, and number of identified peptides of core kinetochore proteins are shown. See Supplementary Table 1 for all proteins identified by mass spectrometry. Ndc10 and Ydr532c are also known as Cbf2 and Kre28, respectively. **d**, Eluted kinetochore particles were subjected to S-500 size exclusion chromatography and analysed by immunoblots. The kinetochore proteins analysed co-migrate as a complex (Stokes radius ~25 nm). Supplementary Fig. 3 shows additional fractions.

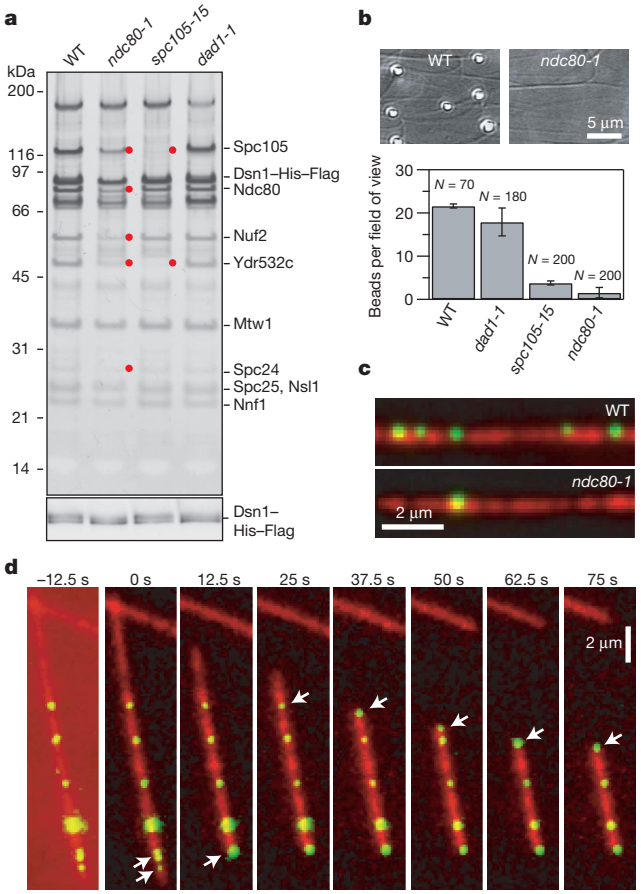

Figure 2 | Purified kinetochore particles bind microtubules *in vitro*. **a**, Silver-stained SDS–PAGE of Dsn1–His–Flag kinetochore material from wild type (WT), *ndc80-1*, *spc105-15* and *dad1-1* mutants. Red dots indicate reduced proteins in the mutant preparations (see Supplementary Fig. 4). Bottom: anti-Flag immunoblot against Dsn1–His–Flag. **b**, Binding of beads prepared with material from indicated strains to taxol-stabilized microtubules (mean ± s.d., from *N* fields, as indicated). **c**, Fluorescence images of Cse4–GFP kinetochore particles (green) from wild-type and *ndc80-1* strains bound to taxol-stabilized microtubules (red). **d**, Selected frames from Supplementary Movie 1 showing movement of Cse4–GFP particles (arrows) driven by the disassembling ends of a microtubule (red; see also Supplementary Fig. 7 and Supplementary Movie 2).

kinetochores *in vivo*. During disassembly, the attachments also moved in a direction opposite the trapping force, demonstrating that they can harness energy stored in the microtubule lattice to produce mechanical work. Notably, their coupling behaviour was more robust than simpler couplers based on recombinant Ndc80 and Dam1 complexes[16–18] (Supplementary Fig. 9), and they formed strong attachments even when the Dsn1:bead ratio was reduced below 200:1 (Fig. 3b, c and Supplementary Fig. 10). Particles from the *dad1-1* mutant strain formed weaker attachments (Fig. 3b, c), whereas those from *ndc80-1* or *spc105-15* strains usually failed to interact detectably with the filaments (similar to the results with taxol-stabilized microtubules) (Fig. 3d).

The robust behaviour of the wild-type kinetochore particles at low Dsn1:bead ratios indicates that few particles, perhaps just one, may be required to form a load-bearing coupler (Supplementary Note 6). If single particles suffice, then under conditions of limiting particle density the strength of the interaction should remain invariant as the density of particles on the beads is reduced. Consistent with this prediction, the force required to rupture attachments associated with growing microtubule ends was statistically indistinguishable, averaging 9.1 ± 0.2 pN, across a 100-fold range of Dsn1:bead ratios (Fig. 3b, c). A second prediction is that the fraction of active beads, $A(c)$, should vary according to the Poisson probability that a bead carries one or more active particles, $A(c) = 1 - e^{-\lambda c}$, where c is the relative Dsn1 concentration and λ is a fitting parameter. Indeed, this form of $A(c)$ matches closely the fraction of beads that formed attachments to growing ends (Fig. 3d). The observation that a measurable event becomes rarer upon dilution while its properties remain unchanged is the hallmark of a 'single molecule' experiment. Analogous observations first demonstrated that single motor enzymes such as kinesin and myosin V are processive, for example in refs 20–22. Here it indicates that robust coupling is an intrinsic and stable property of the purified kinetochore particles — artificial oligomerization on the bead surface is not required. It also demonstrates a close match to the physiological situation in budding yeast, where each individual kinetochore is coupled to the tip of a single microtubule[23].

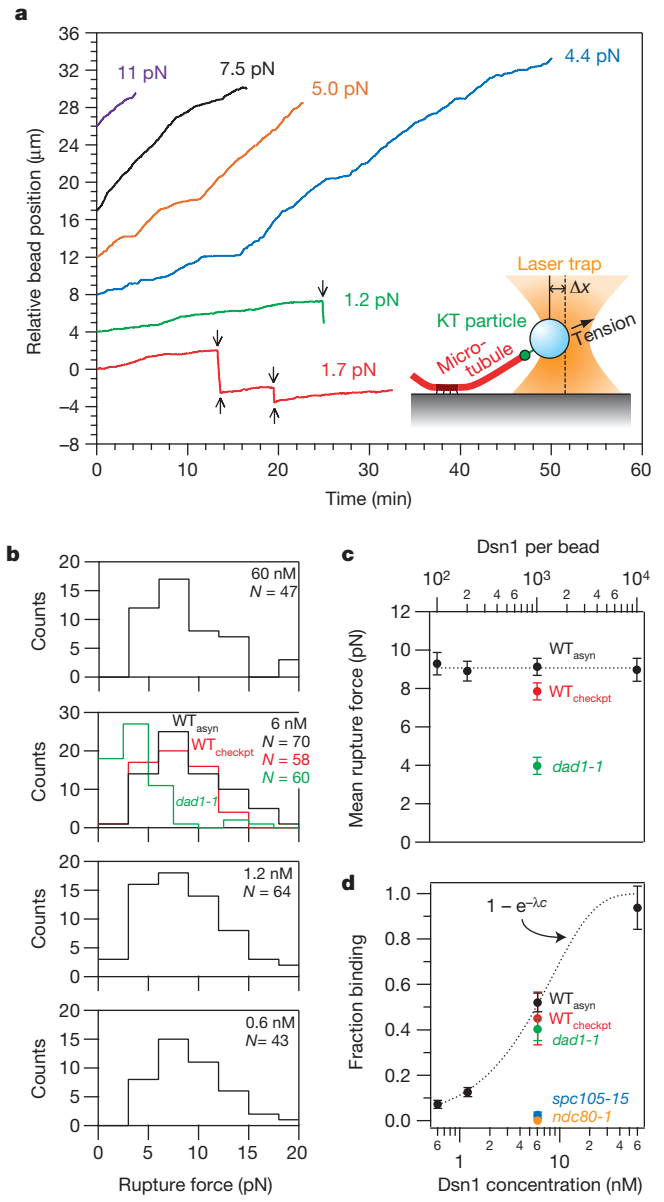

Figure 3 | Single kinetochore particles suffice for robust coupling. **a**, Records of position versus time for native kinetochore-based attachments at indicated tensile loads. Arrows mark transitions (catastrophes and rescues). **b**, Rupture force distributions for beads prepared with particles at indicated concentrations from wild-type (WT_{asyn}), *dad1-1*, and checkpoint-activated wild-type cells ($WT_{checkpt}$). **c**, Mean rupture force (± s.d., from *N* ruptures, indicated in **b**) versus labelling density, expressed as the Dsn1–His–Flag concentration (bottom scale) and the corresponding Dsn1:bead ratio (top scale). **d**, Fraction of beads that bound a growing microtubule end (mean ± s.d., $N = 11$–396). Dotted curve shows Poisson fit (see text and Supplementary Information for details).

The basis for accurate chromosome segregation is thought to be tension-dependent stabilization of bi-oriented kinetochore–microtubule attachments[24]. This selective stabilization has been attributed to an indirect mechanism where tension inhibits phosphorylation of kinetochores by the Aurora B kinase[4,5]. As a first step towards reconstituting this mechanism, we measured the effect of tension on attachment lifetimes for individual end-associated kinetochore particles. Considering that the particles lacked detectable Aurora B (Supplementary Table 1), that there was no ATP present to allow phosphorylation, and that protein–protein interactions are typically destabilized by force[25,26], we expected a monotonic decrease in lifetime with increasing tension. Surprisingly, increasing tension between 1 and 5 pN enhanced the stability of the attachments (Fig. 4a), raising their mean lifetime from 21 ± 5 to 50 ± 17 min ($P = 0.0012$; based on $N = 15$ and 9 events observed for 5.2 and 7.5 h, respectively). This result shows that physiological levels of tension can stabilize kinetochore-microtubule attachments directly, by a mechanism that does not require Aurora B. The result is also reminiscent of 'catch bonds' between receptor–ligand pairs, which enhance cell adhesion in the presence of mechanical force[7–10].

Catch bonds are often explained using two-state kinetic models in which the receptor–ligand pair can switch between a strongly and a weakly bound state, and tension promotes adoption of the strong state[7,9]. Considering that microtubule tips also switch between two states, assembly and disassembly, we thought a similar model might apply to our reconstituted attachments (Fig. 4b). To test this, we measured independently how the rates of the following four events varied with tension: detachment during assembly, detachment during disassembly, catastrophe, and rescue. The detachment rate during assembly was low ($\sim 1\ h^{-1}$) and it increased gradually with tension (Fig. 4c, red). By comparison, detachment during disassembly was much faster (10- to 100-fold) but less sensitive to tension, decreasing with force (Fig. 4c, blue). We speculate that this suppression of detachment may arise from the force-dependent slowing of disassembly (Fig. 4e, blue). Together, the two detachment rates are consistent with a two-state catch bond-like

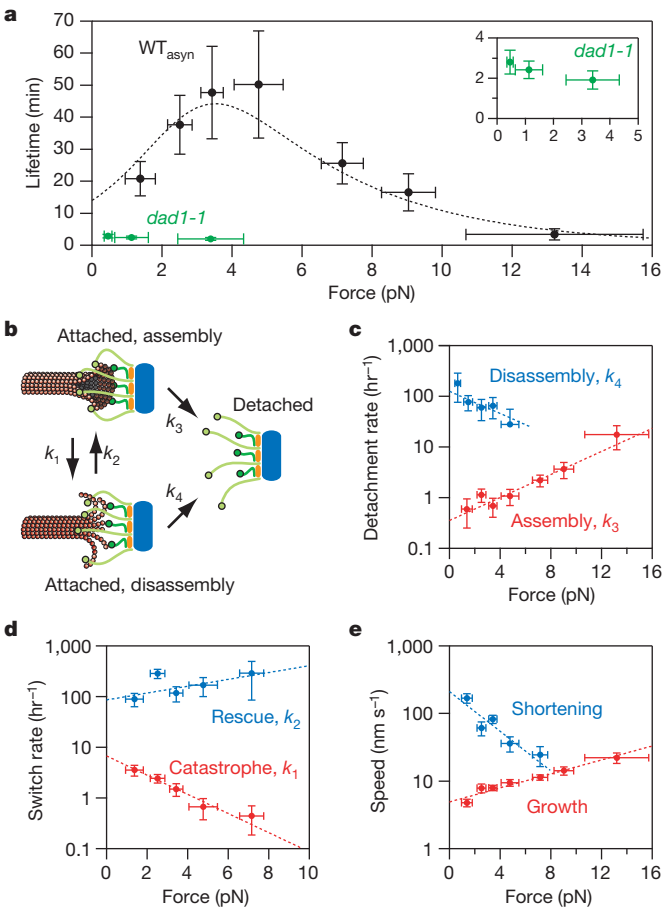

Figure 4 | Tension stabilizes attachments between kinetochore particles and dynamic microtubules. **a**, Measured attachment lifetimes for wild-type (WT_{asyn}) and *dad1-1* particles. Tension initially prolongs and then shortens lifetimes for wild-type attachments. Dotted curve shows prediction of the two-state model (see text). **b**, Schematic of two-state model with detachment during assembly and disassembly (rates k_3 and k_4, respectively), and interconversion between states (k_1 and k_2). **c**–**e**, Measured rates and exponential fits for detachment during assembly (**c**, red), detachment during disassembly (**c**, blue), catastrophe (**d**, red), rescue (**d**, blue), growth (**e**, red) and shortening (**e**, blue). Error bars represent (**a**–**d**) counting uncertainty ($N = 24$–65) and (**e**) s.e.m. ($N = 78$–360).

model in which the strongly- and weakly-bound states correspond to tip assembly and disassembly, respectively. Tension also inhibited catastrophes (Fig. 4d, red) and promoted rescues (Fig. 4d, blue), similar to our previous findings with Dam1-based attachments[17]. The lower catastrophe and higher rescue rates imply that filaments under tension spend less time in the disassembling state, when the kinetochore particles are most vulnerable to detachment. We fit the force-dependence of all four rates with exponential curves (Figs 4c, d and Supplementary Table 2) and, without further fitting, used these to predict the lifetime versus force relationship for the two-state catch bond-like model (Supplementary Note 7). The excellent quantitative agreement with measured lifetimes (see Fig. 4a) confirms that this model can explain the tension-dependent stabilization effect. If an analogous effect occurs at kinetochore–microtubule junctions *in vivo*, it could make an important contribution to the selective stabilization of bi-oriented attachments (see Supplementary Fig. 11).

In summary, our purification of active kinetochore particles has enabled the first direct measurements of the coupling strength between individual native kinetochore particles and dynamic microtubules. Robust coupling at the single particle level depends on the outer microtubule-binding subcomplexes from the budding yeast core kinetochore. Strikingly, tension enhances the stability of these attachments in a manner independent of Aurora B. On this basis we propose that selective stabilization of correct kinetochore–microtubule attachments occurs *in vivo* through a combination of at least two mechanisms, the canonical tension-dependent phosphoregulation, plus a more primitive mechanism based on tension-dependent modulation of tip dynamics.

METHODS SUMMARY

All yeast strains and plasmids used in this study are listed in Supplementary Tables 3 and 4. Media and genetic and microbial techniques were as described[27]. Immunoblotting and SDS–PAGE were as described[28]. Kinetochore particles were isolated by affinity-purifying Dsn1–Flag or Dsn1–His–Flag protein using a modified mini-chromosome purification protocol[11] (see Methods). A typical concentration of Dsn1–Flag or Dsn1–His–Flag was ~4 μg ml^{-1} (60 nM). Size-exclusion chromatography was carried out on a Sephacryl S-500 HR column (Amersham). Estimation of Stokes radii was obtained using a high molecular weight calibration kit (Bio-Rad) and the void volume of the column was determined using 500 nm polystyrene beads (Polysciences). Mass spectrometry was performed as described[11]. Total internal reflection fluorescence (TIRF) microscopy and flow cell preparation were performed as previously described[16,18]. Purified Dsn1–His–Flag kinetochore particles were linked to polystyrene beads via biotinylated anti-penta-His antibody, essentially as described[16]. The laser trap has also been described previously[16–19].

Full Methods and any associated references are available in the online version of the paper at www.nature.com/nature.

Received 13 April; accepted 19 October 2010.

1. Santaguida, S. & Musacchio, A. The life and miracles of kinetochores. *EMBO J.* **28,** 2511–2531 (2009).
2. Cheeseman, I. M. & Desai, A. Molecular architecture of the kinetochore-microtubule interface. *Nature Rev. Mol. Cell Biol.* **9,** 33–46 (2008).
3. Nicklas, R. B. The forces that move chromosomes in mitosis. *Annu. Rev. Biophys. Biophys. Chem.* **17,** 431–449 (1988).
4. Maresca, T. J. & Salmon, E. D. Welcome to a new kind of tension: translating kinetochore mechanics into a wait-anaphase signal. *J. Cell Sci.* **123,** 825–835 (2010).
5. Liu, D., Vader, G., Vromans, M. J., Lampson, M. A. & Lens, S. M. Sensing chromosome bi-orientation by spatial separation of aurora B kinase from kinetochore substrates. *Science* **323,** 1350–1353 (2009).
6. Straight, A. F., Marshall, W. F., Sedat, J. W. & Murray, A. W. Mitosis in living budding yeast: anaphase A but no metaphase plate. *Science* **277,** 574–578 (1997).
7. McEver, R. P. & Zhu, C. Rolling cell adhesion. *Annu. Rev. Cell Dev. Biol.* **26,** 363–396 (2010).
8. Sarangapani, K. K. *et al.* Low force decelerates L-selectin dissociation from P-selectin glycoprotein ligand-1 and endoglycan. *J. Biol. Chem.* **279,** 2291–2298 (2004).
9. Thomas, W. E., Vogel, V. & Sokurenko, E. Biophysics of catch bonds. *Annu Rev Biophys* **37,** 399–416 (2008).
10. Marshall, B. T. *et al.* Direct observation of catch bonds involving cell-adhesion molecules. *Nature* **423,** 190–193 (2003).
11. Akiyoshi, B., Nelson, C. R., Ranish, J. A. & Biggins, S. Quantitative proteomic analysis of purified yeast kinetochores identifies a PP1 regulatory subunit. *Genes Dev.* **23,** 2887–2899 (2009).
12. De Wulf, P., McAinsh, A. D. & Sorger, P. K. Hierarchical assembly of the budding yeast kinetochore from multiple subcomplexes. *Genes Dev.* **17,** 2902–2921 (2003).
13. Nekrasov, V. S., Smith, M. A., Peak-Chew, S. & Kilmartin, J. V. Interactions between centromere complexes in *Saccharomyces cerevisiae*. *Mol. Biol. Cell* **14,** 4931–4946 (2003).
14. Cheeseman, I. M., Chappie, J. S., Wilson-Kubalek, E. M. & Desai, A. The conserved KMN network constitutes the core microtubule-binding site of the kinetochore. *Cell* **127,** 983–997 (2006).
15. Tanaka, K. *et al.* Molecular mechanisms of kinetochore capture by spindle microtubules. *Nature* **434,** 987–994 (2005).
16. Powers, A. F. *et al.* The Ndc80 kinetochore complex forms load-bearing attachments to dynamic microtubule tips via biased diffusion. *Cell* **136,** 865–875 (2009).
17. Franck, A. D. *et al.* Tension applied through the Dam1 complex promotes microtubule elongation providing a direct mechanism for length control in mitosis. *Nature Cell Biol.* **9,** 832–837 (2007).
18. Tien, J. F. *et al.* Cooperation of the Dam1 and Ndc80 kinetochore complexes enhances microtubule coupling and is regulated by aurora B. *J. Cell Biol.* **189,** 713–723 (2010).
19. Franck, A. D., Powers, A. F., Gestaut, D. R., Davis, T. N. & Asbury, C. L. Direct physical study of kinetochore-microtubule interactions by reconstitution and interrogation with an optical force clamp. *Methods* **51,** 242–250 (2010).
20. Howard, J., Hudspeth, A. J. & Vale, R. D. Movement of microtubules by single kinesin molecules. *Nature* **342,** 154–158 (1989).
21. Block, S. M., Goldstein, L. S. & Schnapp, B. J. Bead movement by single kinesin molecules studied with optical tweezers. *Nature* **348,** 348–352 (1990).
22. Mehta, A. D. *et al.* Myosin-V is a processive actin-based motor. *Nature* **400,** 590–593 (1999).
23. Winey, M. *et al.* Three-dimensional ultrastructural analysis of the *Saccharomyces cerevisiae* mitotic spindle. *J. Cell Biol.* **129,** 1601–1615 (1995).
24. Nicklas, R. B. & Ward, S. C. Elements of error correction in mitosis: microtubule capture, release, and tension. *J. Cell Biol.* **126,** 1241–1253 (1994).
25. Bell, G. I. Models for the specific adhesion of cells to cells. *Science* **200,** 618–627 (1978).
26. Merkel, R., Nassoy, P., Leung, A., Ritchie, K. & Evans, E. Energy landscapes of receptor-ligand bonds explored with dynamic force spectroscopy. *Nature* **397,** 50–53 (1999).
27. Rose, M. D., Winston, F. & Heiter, P. Methods in yeast genetics. (Cold Spring Harbor Laboratory Press, 1990).
28. Biggins, S. *et al.* The conserved protein kinase Ipl1 regulates microtubule binding to kinetochores in budding yeast. *Genes Dev.* **13,** 532–544 (1999).

Supplementary Information is linked to the online version of the paper at www.nature.com/nature.

Acknowledgements We thank A. Desai for antibodies, and J. Kilmartin, G. Barnes, D. Pellman, R. Tsien and the Yeast Resource Center for strains and plasmids. We also thank M. Press for constructing the Cse4–GFP strain, M. Yuan at the ISB for help, and the Seattle Mitosis Club for comments. We are grateful to T. Davis, W. Thomas, B. Zagotta, T. Tsukiyama, J. Stumpff, F. Rieke, S. Gordon and the Biggins lab for comments on the manuscript. This work was supported by an NSF IGERT fellowship (DGE-0504573) and NIH traineeship (T32GM07270) to A.F.P., an NIH Cardiovascular Pathology traineeship (T32HL007312) to K.K.S., a Beckman Young Investigator grant to S.B., NIH grants (GM078069 and GM064386) to S.B., an NCI Cancer Center Support grant (CA015704) and an NIGMS grant (PM50 GM076547/Center for Systems Biology) to J.A.R., a Searle Scholar Award (06-L-111) to C.L.A., a Packard Fellowship for Science and Engineering (2006-30521) to C.L.A. and an NIGMS grant (R01GM79373) to C.L.A. S.B. is a Scholar of the Leukemia and Lymphoma Society and T.G. is a Howard Hughes Medical Institute Early Career Scientist.

Author Contributions All authors designed various components of the research. B.A. and C.R.N. constructed plasmids and yeast strains and B.A. purified kinetochore particles and analysed composition. B.A. and J.A.R. performed mass spectrometry and data analysis. A.F.P., K.K.S., H.A.S. and C.L.A. performed microtubule experiments. S.L.R. performed gel filtration.

Author Information Reprints and permissions information is available at www.nature.com/reprints. The authors declare no competing financial interests. Readers are welcome to comment on the online version of this article at www.nature.com/nature. Correspondence should be addressed to S.B. (sbiggins@fhcrc.org) or C.L.A. (casbury@u.washington.edu) and requests for materials to S.B.

METHODS

Yeast strains, plasmids and microbial techniques. Media and genetic and microbial techniques were essentially as described[27]. Mitotic cultures were prepared with benomyl as described[11]. For temperature-sensitive mutants, cells were shifted to 37 °C for 3 h. Yeast strains and plasmids used in this study are listed in Supplementary Tables 3 and 4. The *ndc80-1* (ref. 29), *spc105-15* (ref. 13), *SPC105–GFP* (ref. 13), *YDR532c–GFP* (ref. 13), *dad1-1* (ref. 30) alleles were crossed to make strains for this study. Strains containing *NUF2–3GFP:His3* and *CSE4–GFP:URA3* were made by integrating plasmid pSB897 digested with XcmI at the *NUF2* locus and pSB1617 digested with StuI at the *URA3* locus, respectively. Deletions, as well as 3Flag, 13Myc and mCherry epitope tags were made using a PCR-based integration system and confirmed by PCR[31–33]. The 6His–3Flag epitope tagging of the endogenous *DSN1* gene was performed using a PCR-based integration system using primers SB2434-SB2435 and plasmid pSB1590 as a template. All tagged strains we constructed are functional *in vivo* and do not cause any detectable growth defects or temperature sensitivity. Specific primer sequences are available on request.

Plasmid construction. pSB1590 (*DSN1-6His–3Flag*, *URA3*, integrating vector) was constructed in multiple steps as follows. First, pSB1110 (*DSN1-12Myc*, *URA3*, integrating vector) was made by amplification of *DSN1* from pSB624 (*DSN1*, *CEN*, *URA3*)[34] using primers SB1675 and SB1676. The PCR product was digested with XhoI and EcoRI and ligated into the same sites in pSB167 (*12Myc*, *URA3*, integrating vector)[28]. Second, a DNA fragment encoding *3Flag* with 5′ EcoRI and 3′ XmaI sites engineered was made by annealing SB1698 and SB1699. The fragment was then integrated just before the *12myc* open reading frame of pSB1110 (*DSN1-12Myc*, *URA3*, integrating vector) that was digested with EcoRI and XmaI to make pSB1113 (*DSN1–3Flag*, *URA3*, integrating vector). Finally, to make pSB1590 (*DSN1–6His–3Flag*, *URA3*, integrating), a DNA fragment encoding the *6His* tag with EcoRI sites at both ends was made by annealing SB2432 and SB2433, which was then integrated just before *3Flag* of pSB1113 using EcoRI. The Nuf2–3GFP (pSB897) was made by PCR amplification of the carboxy-terminal 853 base pairs of *NUF2* using primers SB1124 and SB1125 that have EcoRI and BamHI restriction sites engineered, respectively. The resulting PCR product was digested with EcoRI–BamHI and ligated into the same sites of pSB623 (gift of D. Pellman). To make Cse4–GFP (pSB1617), *GFP* was amplified by PCR from pSB623 using primers SB2443 and SB2444, digested with XbaI, and integrated into the XbaI site of pSB241 (*CSE4*, *URA3*, integrating vector)[35]. pSB1265 (*3Flag*, *TRP1*) was made by replacing *KAN* marker gene of pSB812 (*3Flag*, *KAN*) with *TRP1* marker gene from pSB450 (*TRP1*) using SpeI and SalI. pSB1643 (glutathione *S*-transferase fusion GST-N-Spc105 expression vector) was made by PCR amplification of the amino-terminal 798 bp of *SPC105* using primers SB2590 and SB2591 that have BamHI and EcoRI sites engineered, respectively. The resulting PCR product was digested with BamHI–EcoRI and ligated into the same sites of pGEX-2T (Amersham).

Isolation of kinetochore particles. Kinetochore particles were isolated by affinity-purifying Dsn1–Flag or Dsn1–His–Flag protein using a minichromosome purification protocol[11] with the following modifications. Briefly, cells were grown in complete YPD (yeast extract, peptone, dextrose) media and extract was prepared by breaking cells in a blender with dry ice, followed by ultracentrifugation. Beads conjugated with anti-Flag antibodies were incubated with extract for 3 h with constant rotation, followed by four washes with buffer H (BH)/0.15 (25 mM HEPES pH 8.0, 2 mM $MgCl_2$, 0.1 mM EDTA pH 8.0, 0.5 mM EGTA pH 8.0, 0.1% NP-40, 150 mM KCl, 15% glycerol) containing protease inhibitors, phosphatase inhibitors and 2 mM dithiothreitol (DTT). Beads were further washed twice with BH/0.15 with protease inhibitors. Associated proteins were eluted from the beads by gentle agitation of beads in elution buffer (0.5 mg ml^{-1} 3Flag peptide in BH/0.15 with protease inhibitors) for 25 min at room temperature. A typical concentration of Dsn1–Flag or Dsn1–His–Flag was ~4 μg ml^{-1} (60 nM) as determined by comparing the purified material with BSA standards on silver-stained SDS–PAGE gels. Similar results were obtained using SYPRO Ruby dye. Aliquots were made and stored at −80 °C. Typically, 2 l of asynchronously growing culture were used for microtubule-binding experiments, 24 l of mitotic culture for S-500 gel filtration experiments. Based on silver-stained SDS–PAGE, the composition of the kinetochore particles purified from mitotically arrested cells does not differ detectably from particles purified from asynchronous cultures. This finding is consistent with the observation that budding yeast kinetochores bind microtubules throughout most of the cell cycle[36]. To identify co-purifying proteins, associated proteins were eluted with detergent and analysed by mass spectrometry as described[11].

Protein and immunological techniques. Immunoblotting was performed as described[28]. Anti-Spc105 (1–266 amino acid) polyclonal antibodies were raised and affinity purified using pSB1643 (GST-N-Spc105) as previously described[34] and used at a 1:1,000 dilution. Anti-Flag antibodies (Sigma-Aldrich) were used at 1:3,000 and anti-Cse4 antibodies at 1:500 (ref. 34). Anti-Ndc80 (OD4, 1:10,000), anti-Ndc10 (OD1, 1:5,000), anti-Mif2 (OD2, 1:6,000), and anti-Ctf19 (OD10, 1:15,000) antibodies were generous gifts from A. Desai[11]. To compare microtubule binding activity between different kinetochore mutants, the concentration of Dsn1–Flag was normalized by quantifying its signal intensity using the Odyssey infrared imaging system (Li Cor Bioscience). Silver-staining was performed on 4–12% NuPAGE Novex Bis-Tris gels (Invitrogen) using a SilverQuest silver-staining kit according to instructions (Invitrogen). Size-exclusion chromatography was carried out on a Sephacryl S-500 HR column (Amersham) equilibrated in BH/0.15 at 4 °C. Estimation of Stokes radii was obtained using a high-molecular weight calibration kit (Bio-Rad) and the void volume of the column was determined using 500 nm polystyrene beads (Polysciences).

TIRF microscopy. We used a custom TIRF microscope and flow cell preparation that has been previously described[16,18,37]. After an initial rinse with 0.3 ml double distilled H_2O, 'rigor' kinesin[38] diluted in BRB80 (80 mM PIPES, 1 mM $MgCl_2$, 1 mM EGTA at pH 6.9) containing 1 mg ml^{-1} κ-casein and 10 μM taxol (BCT) was introduced and allowed to bind for 5 min. Unbound kinesin was removed with 100 μl BCT, and Alexa 647-labelled taxol microtubules diluted in BCT plus oxygen scavengers (BCTscavs; 200 μg ml^{-1} glucose oxidase, 25 mM glucose, 35 μg ml^{-1} catalase and 5 mM DTT) were introduced and allowed to bind to the desired density. Flow cells were then washed with 50 μl BCTscavs, and fluorescent kinetochore particles (diluted in BCTscavs) were introduced and given 5 min to bind.

For experiments using dynamic microtubules, Alexa 647-labelled GMPCPP (guanylyl-(alpha,beta)-methylene-diphosphonate) microtubules were bound to coverslip-adsorbed rigor kinesin, washed with 50 μl warm growth buffer (BRB80, 1 mg ml^{-1} κ-casein, 1 mM GTP, 200 μg ml^{-1} glucose oxidase, 25 mM glucose, 35 μg ml^{-1} catalase and 5 mM DTT) and then incubated with growth buffer supplemented with 2 mg ml^{-1} Alexa 647 tubulin (1% labelled) and fluorescent kinetochore particles. Dynamic extensions were grown for ~5 min at 30 °C, after which depolymerization was triggered by exchanging for tubulin-free buffer.

Assay for bead binding to taxol-stabilized microtubules. Purified Dsn1–His–Flag kinetochore particles were diluted in BRB80 plus 1 mg ml^{-1} κ-casein and linked to polystyrene beads via biotinylated anti-penta-His antibody, essentially as described in ref. 16. Flow cells (described in ref. 19) were treated with taxol-stabilized microtubules, which non-specifically adsorb to the coverslip surface, and then blocked with BCT for 10 min before the introduction of kinetochore particle-coated beads. After a 10 min incubation to allow for binding, the flow cells were imaged in DIC and the number of microtubule-bound beads per field of view was counted. Binding was negligible (2 beads in 150 fields) in negative controls using beads lacking the anti-penta-His antibody, prepared with wild-type kinetochore material at an equivalent Dsn1:bead ratio (100:1).

Constant-force laser trap assays. To determine if bead-bound kinetochore particles can couple physiologically relevant forces to dynamic microtubule tips, we used a laser trapping-based motility assay[16–19,39]. Dynamic microtubule extensions were grown from coverslip-anchored GMPCPP-stabilized microtubule seeds in a buffer consisting of BRB80, 1 mg ml^{-1} κ-casein, 1 mM GTP, 250 μg ml^{-1} glucose oxidase, 25 mM glucose, 30 μg ml^{-1} catalase, 1 mM DTT and 1.5 mg ml^{-1} purified bovine brain tubulin. Assays were performed at 23 °C.

The laser trap has been described previously[19]. Position sensor response was mapped using the piezo stage to raster-scan a stuck bead through the beam, and trap stiffness was calibrated along the two principle axes using the drag force, equipartition and power spectrum methods. Force feedback was implemented with custom LabView software. During clamping of the force, bead-trap separation was sampled at 40 kHz while stage position was updated at 50 Hz to maintain the desired load. Bead and stage position data were decimated to 200 Hz before storing to disk.

All the wild-type kinetochore particle data shown in Figs 3a, 4 and Supplementary Fig. 9 were recorded using beads prepared at a Dsn1:bead ratio of 200:1 (1.2 nM Dsn1–His–Flag, 5.6 pM beads), well below the single particle limit. The statistics for kinetochore particles presented in Supplementary Fig. 9a, b were calculated from a set of 40 individual events, lasting a total of 11.5 h, during which the particles were subjected to a constant tensile force of 1.9 ± 0.4 pN (mean ± s.d.). Event duration and travel distance were computed from the instant an attachment was fully loaded until the event ended, often due to bead detachment but sometimes for other reasons (for example, when another bead fell into the trap). All individual event durations and travel distances were averaged, irrespective of how the events ended.

The data for wild-type particles in Fig. 4a and 4c–e were calculated from a set of 170 individual events, lasting a total of 42.5 h, during which the kinetochore particles were subjected to constant tensile forces between 0.3 and 18 pN. This data set included all events used for Fig. 3a and Supplementary Fig. 9, plus an additional 130 events recorded to investigate microtubule dynamics and attachment lifetimes as functions of force. Lifetimes (Fig. 4a) were computed by summing the total time of all events in a given force range and dividing by the number of detachments in that range. Rates of detachment during assembly (Fig. 4c, red) and catastrophe (Fig. 4d, red) were computed by counting the numbers of these events

in a given force range and dividing by the total assembly time in that range. Likewise, rates of detachment during disassembly (Fig. 4c, blue) and rescue (Fig. 4d, blue) were computed by counting events and dividing by the total disassembly time in each force range.

Rupture force measurements. Beads were prepared with kinetochore material at molar ratios ranging from 100 to 10,000 Dsn1 molecules per bead. Individual beads were attached to the ends of growing microtubules and preloaded with a constant tension of 1.1 ± 0.1 pN for the *dad1-1* mutants, or 3.8 ± 0.2 pN for the wild-type kinetochore particles. The laser trap was programmed to subsequently ramp the force at a defined rate (0.25 pN s^{-1}) until the linkage ruptured or the load limit of the trap was reached (20 pN) and the bead escaped from the trap. At all but the highest densities of kinetochore material (that is, below 60 nM Dsn1–His–Flag), a small fraction (~14%) of the beads escaped the trap. Escape was ~threefold more likely at 60 nM Dsn1–His–Flag, suggesting that load might be shared by multiple particles at high densities. Note that for the Poisson probability curve in Fig. 4c, the fitting parameter λ accounts for both the number of Dsn1 molecules per particle and the proportion of particles that are geometrically inaccessible to the microtubule, or otherwise inactive.

29. Wigge, P. A. *et al.* Analysis of the *Saccharomyces* spindle pole by matrix-assisted laser desorption/ionization (MALDI) mass spectrometry. *J. Cell Biol.* **141,** 967–977 (1998).
30. Enquist-Newman, M. *et al.* Dad1p, third component of the Duo1p/Dam1p complex involved in kinetochore function and mitotic spindle integrity. *Mol. Biol. Cell* **12,** 2601–2613 (2001).
31. Longtine, M. S. *et al.* Additional modules for versatile and economical PCR-based gene deletion and modification in *Saccharomyces cerevisiae*. *Yeast* **14,** 953–961 (1998).
32. Gelbart, M. E., Rechsteiner, T., Richmond, T. J. & Tsukiyama, T. Interactions of Isw2 chromatin remodeling complex with nucleosomal arrays: analyses using recombinant yeast histones and immobilized templates. *Mol. Cell. Biol.* **21,** 2098–2106 (2001).
33. Sikorski, R. S. & Hieter, P. A system of shuttle vectors and yeast host strains designed for efficient manipulation of DNA in *Saccharomyces cerevisiae*. *Genetics* **122,** 19–27 (1989).
34. Pinsky, B. A., Tatsutani, S. Y., Collins, K. A. & Biggins, S. An Mtw1 complex promotes kinetochore biorientation that is monitored by the Ipl1/Aurora protein kinase. *Dev. Cell* **5,** 735–745 (2003).
35. Buvelot, S., Tatsutani, S. Y., Vermaak, D. & Biggins, S. The budding yeast Ipl1/Aurora protein kinase regulates mitotic spindle disassembly. *J. Cell Biol.* **160,** 329–339 (2003).
36. Kitamura, E., Tanaka, K., Kitamura, Y. & Tanaka, T. U. Kinetochore microtubule interaction during S phase in *Saccharomyces cerevisiae*. *Genes Dev.* **21,** 3319–3330 (2007).
37. Gestaut, D. R., Cooper, J., Asbury, C. L., Davis, T. N. & Wordeman, L. Reconstitution and functional analysis of kinetochore subcomplexes. *Methods Cell Biol.* **95,** 641–656 (2010).
38. Rice, S. *et al.* A structural change in the kinesin motor protein that drives motility. *Nature* **402,** 778–784 (1999).
39. Asbury, C. L., Gestaut, D. R., Powers, A. F., Franck, A. D. & Davis, T. N. The Dam1 kinetochore complex harnesses microtubule dynamics to produce force and movement. *Proc. Natl Acad. Sci. USA* **103,** 9873–9878 (2006).

doi:10.1038/nature09594

1. Supplementary figures and legends

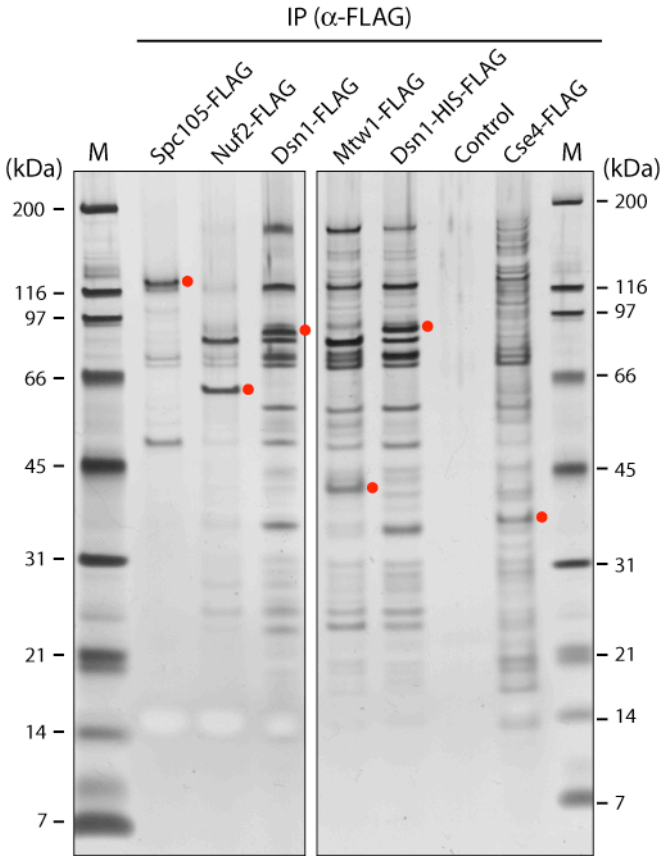

Figure S1. Affinity-purification of various kinetochore subcomplexes.

The indicated Flag-tagged kinetochore proteins (Flag: 4 kDa) were purified using anti-Flag antibodies, eluted with Flag peptide and analyzed by SDS-PAGE followed by silver-staining. An untagged strain was used as a control. Purification of Mis12 kinetochore subcomplex components (Mtw1, Dsn1) isolates most core kinetochore proteins while purifications of the Spc105, Nuf2, and Cse4 proteins under similar conditions do not. Red circles indicate epitope-tagged proteins.

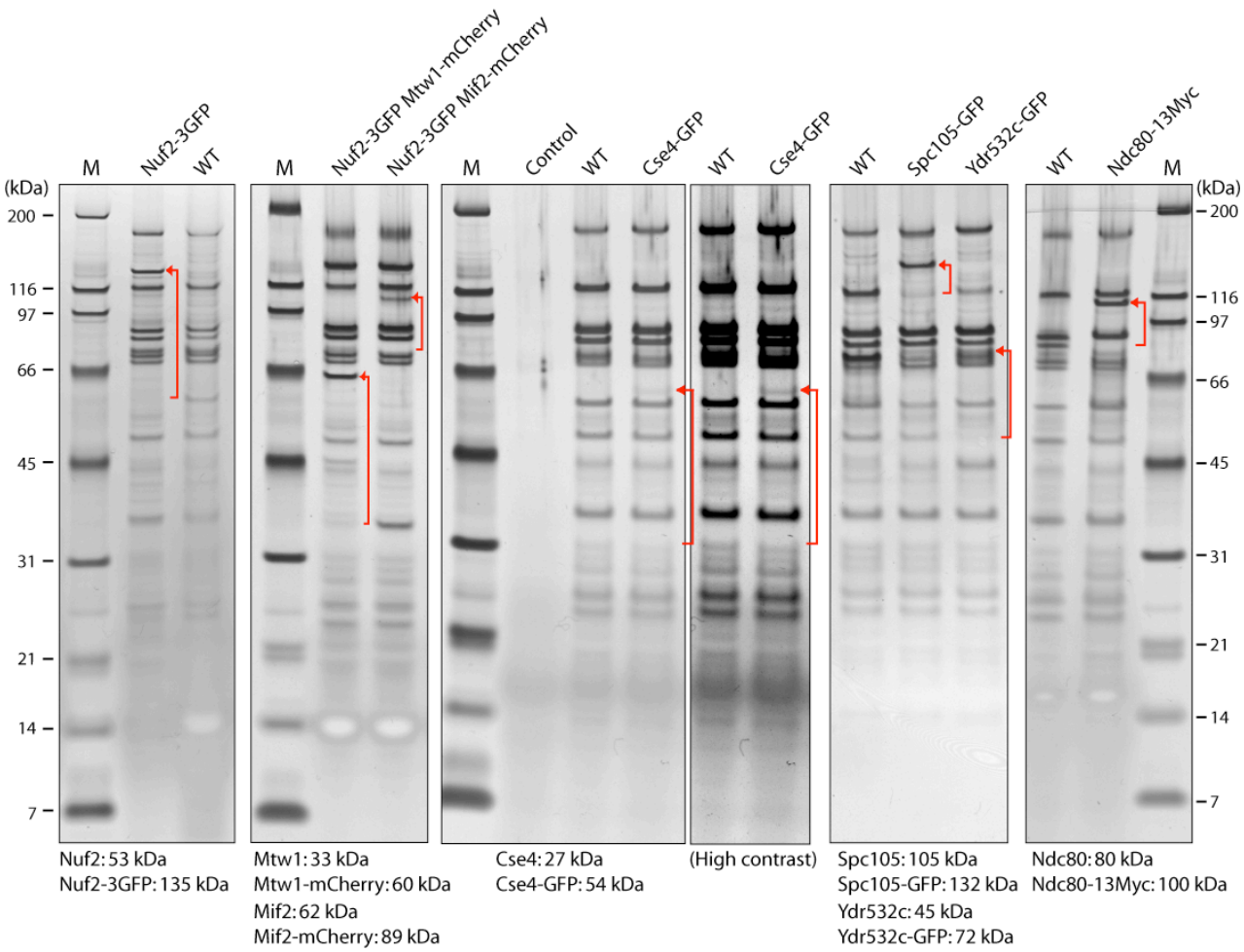

Figure S2. Determination of the composition of purified kinetochore particles.

Kinetochore particles were purified using Dsn1-Flag from strains expressing the indicated fusion proteins. Band shifts (disappearance and appearance of bands marked by red arrows) by predicted molecular weights (1GFP: 27 kDa, 3GFP: 82 kDa, mCherry: 27 kDa, 13Myc: 20 kDa) identify the tagged proteins. KMN (KNL1/Spc105, Mis12, Ndc80 subcomplexes) components are the most abundant proteins in the sample, while Cse4, Mif2 and components of the ten-subunit Dam1 complex (not shown) appear to be present in substoichiometric ratios to KMN.

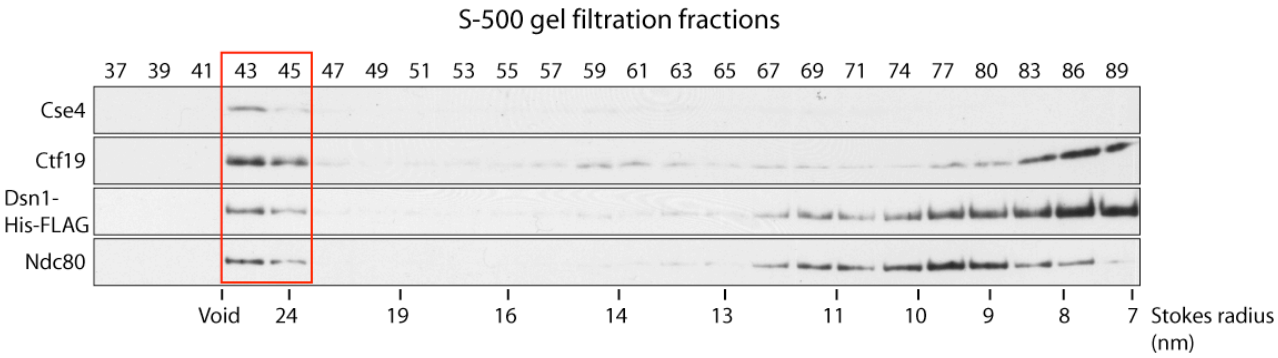

Figure S3. Analysis of S-500 gel filtration fractions over a wide range.

Purified Dsn1-His-Flag samples were analyzed by immunoblotting against the indicated kinetochore proteins after S-500 size exclusion chromatography (fraction numbers indicated above blots). Note that the reported Stokes radius for the Ndc80 subcomplex is ~9 nm, Mis12 complex ~7 nm, COMA ~6 nm[1,2]. The wide distribution of kinetochore proteins could reflect multiple species within the cell and/or deterioration of complexes prior to, or during, the chromatography.

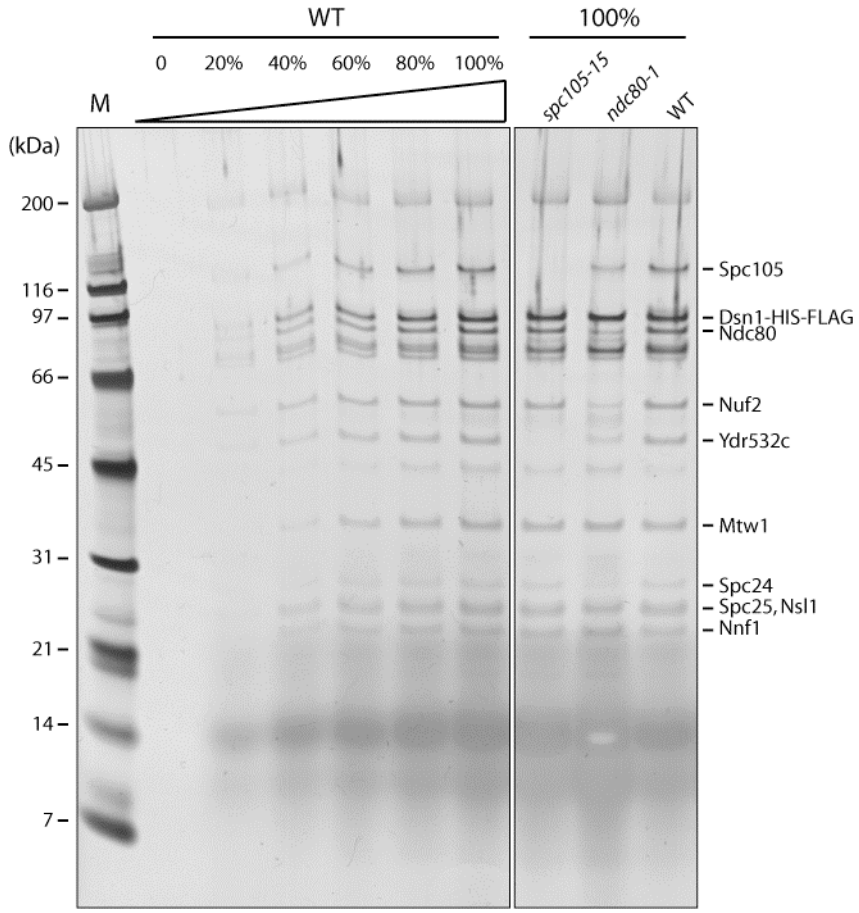

Figure S4. Composition of *ndc80-1* and *spc105-15* mutant kinetochore particles.

Kinetochore particles purified from WT, *ndc80-1,* and *spc105-15* cells were analyzed by SDS-PAGE followed by silver-staining. Serial dilutions of WT sample were loaded to determine the amount of specific kinetochore proteins in the mutant purifications relative to WT. We estimate that kinetochore material purified from *spc105-15* mutant cells contains ~80% of Ndc80 and Nuf2, and <20% of Spc105-15 and Ydr532c, relative to WT. The material from *ndc80-1* mutant cells appears to contain ~30% of Ndc80-1 and Nuf2, and ~45% of Spc105 and Ydr532c.

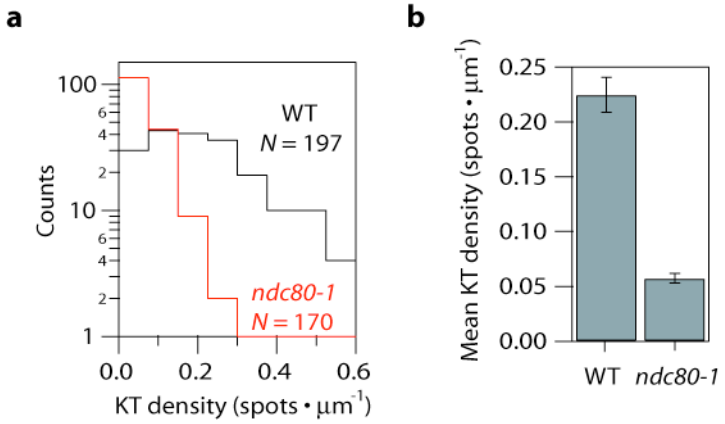

Figure S5. Ndc80-dependent binding of fluorescent kinetochore particles to taxol-stabilized microtubules.

Purified kinetochore particles from strains containing Cse4-GFP were incubated with fluorescent, taxol-stabilized microtubules at a concentration low enough to allow resolution of individual fluorescent particles (1 nM Dsn1-Flag), as shown in Fig 2c. **a**, Distributions showing the number of Cse4-GFP kinetochore particles bound per unit-length microtubule for wild-type (WT, black) and *ndc80-1* (red) particles. **b**, On average, wild-type Cse4-GFP kinetochore particles exhibited ~4-fold greater binding than *ndc80-1* particles. Bars represent mean ± s.e.m., computed from the data in (**a**).

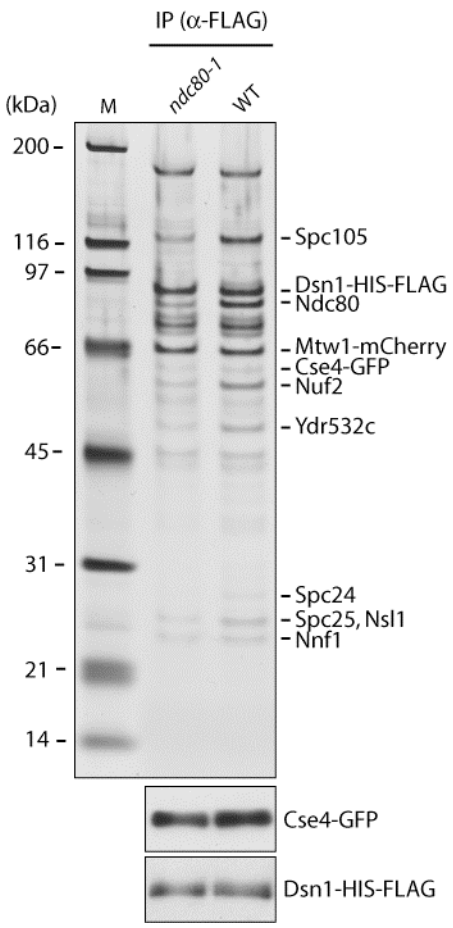

Figure S6. Cse4-GFP is present in the kinetochore particles purified from *ndc80-1* mutant cells.

Kinetochore particles were purified from *NDC80* (WT) or *ndc80-1* cells expressing Cse4-GFP. Purified samples were analyzed by SDS-PAGE followed by silver-staining (top) as well as by immunoblots against Cse4 and Dsn1-His-Flag (bottom).

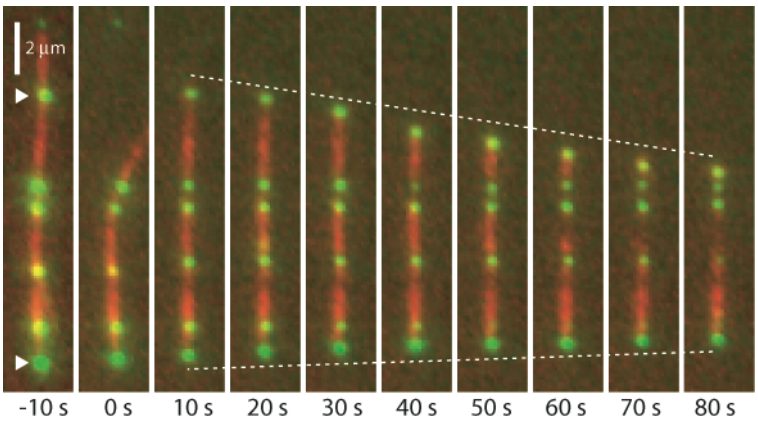

Figure S7. Disassembly-driven movement of Nuf2-3GFP kinetochore particles.

Selected frames from Movie S2 showing processive movement of Nuf2-3GFP kinetochore particles (green spots identified by arrowheads) on the ends of a shortening microtubule (red filament). Microtubules were polymerized from Alexa 647 tubulin in the presence of kinetochore particles (at 0.6 nM Dsn1-Flag). Depolymerization was induced by rapid dilution of free tubulin at t = 0 seconds (dotted lines indicate period of disassembly).

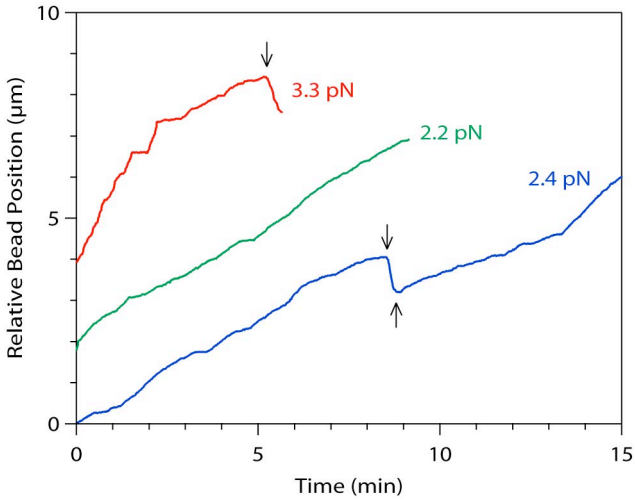

Figure S8. Additional example traces showing that kinetochore particles can couple tension to dynamic microtubules.

Records of position versus time for native kinetochore-based attachments subjected continuously to the indicated level of tensile force. Increasing position represents movement associated with microtubule assembly and decreasing position represents movement driven by disassembly. Arrows mark transitions in growth state (i.e., catastrophe and rescue). For clarity, traces are offset vertically by an arbitrary amount. These data were recorded using kinetochore particles after S-500 size exclusion chromatography (fraction #44, Figs. 1d and S3).

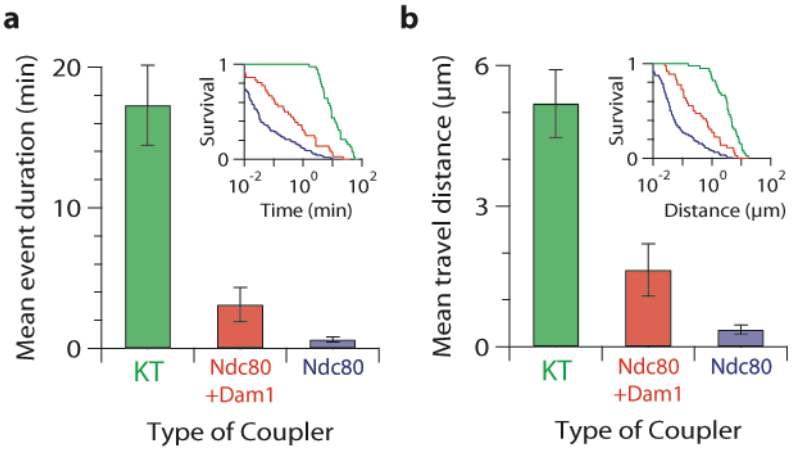

Figure S9. Coupling by kinetochore particles is more robust than simpler couplers based on recombinant Ndc80 and Dam1 subcomplexes.

a and **b**, Average event duration (**a**) and travel distance (**b**) for native kinetochore-based couplers, for couplers composed of bead-bound Ndc80 complexes alone, and for bead-bound Ndc80 in the presence of free Dam1 complex, undergoing assembly- and disassembly-coupled movement under tensile force. Bars represent mean ± s.e.m. Insets show survival probability for native kinetochore-based couplers (green trace), for couplers composed of bead-bound Ndc80 complex alone (blue trace), and for bead-bound Ndc80 in the presence of free Dam1 complex (red trace). $N = 40$, 37, and 112 events, respectively. Data for native kinetochore-based couplers were recorded at 1.9 ± 0.4 pN (mean ± s.d.), using beads prepared at a Dsn1:bead ratio of 200:1 (1.2 nM Dsn1-His-Flag, 5.6 pM beads). Data for recombinant subcomplexes[3] were recorded at 1.8 ± 0.4 pN (mean ± s.d.), using beads with >2,000 Ndc80:bead (>13 nM Ndc80 complex, 6 pM beads), in the absence and presence of ~10 nM Dam1 complex.

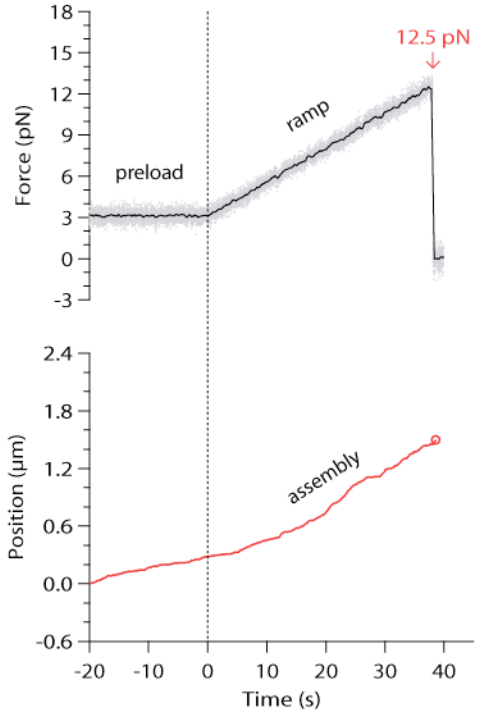

Figure S10. Measurement of rupture force for a bead-bound kinetochore particle attached to an assembling microtubule.

Representative record showing tensile force (upper plot) and position (lower plot) versus time for a bead associated with the assembling tip of a microtubule. The instrument was programmed to automatically ramp the force at a constant rate (0.25 pN s^{-1}) after a brief preload period (during which the force was held constant). Arrow marks maximum force, recorded when the attachment ruptured. Circle marks rupture on lower plot. For this particular event, the beads were prepared with kinetochore particles at a Dsn1:bead ratio of 200:1 (1.2 nM Dsn1-His-Flag, 5.6 pM beads).

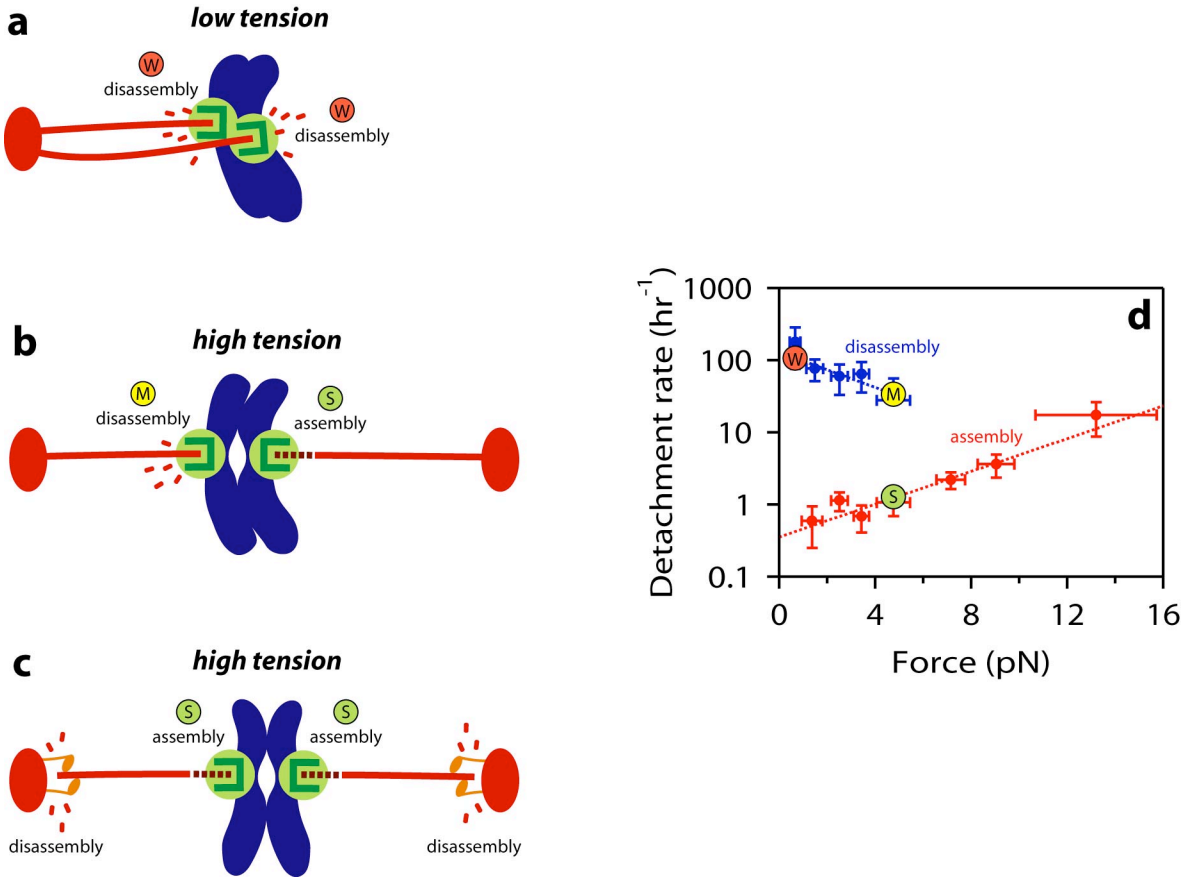

Figure S11. How tension-dependent modulation of tip dynamics could help selectively stabilize bi-oriented attachments *in vivo*.

a - c, For simplicity, we consider three scenarios where the sister kinetochores (large green circles) on a pair of sister chromatids (blue) are each attached to single microtubule tips (red filaments). Qualitatively similar behavior is expected for larger kinetochores that bind multiple tips. **a**, 'syntelic' case. Both sister kinetochores are attached to the tips of microtubules that emanate from the same spindle pole (large red ovals represent poles). Opposing spindle forces do not develop, so tension at both attachments is low. Both tips remain in the disassembling state and, consequently, both attachments are weak (marked here and in **d** by 'W' in small red circle). **b**, 'bi-oriented' case without poleward

flux. Sister kinetochores are attached correctly to the tips of microtubules emanating from opposite sides of the spindle, which generates high tension. The right tip is assembling, so the right attachment is strong ('S' in small green circle). The left tip is disassembling, so the left kinetochore is more vulnerable to detachment than its sister. However, relative to the kinetochores in **a**, it is moderately stabilized ('M' in yellow circle) because tension moderately inhibits detachment during disassembly (as shown in **d**, and in Fig. 4c). **c**, 'bi-oriented' case with poleward flux. Kinetochores attach tips from opposite sides, generating tension as in **b**. In this case, however, continuous poleward flux of the microtubules occurs, driven by traction forces (orange motors) and balanced by disassembly at the poles. Poleward flux allows simultaneous and persistent assembly of both kinetochore-attached tips, so both kinetochores are strongly attached. **d**, Data and fits from Fig. 4c with markers indicating hypothetical detachment rates for the kinetochores in **a** – **c** (assuming forces of ~0.5 and ~5 pN for syntelic and bi-oriented attachments, respectively). Given these detachment rates, the probability for scenario **a** to revert to a singly-attached ('monotelic') state would be 6-fold higher than scenario **b**, and 100-fold higher than scenario **c**. Thus, in either scenario selective stabilization of bi-oriented attachments would occur.

2. Supplementary Notes

Note S1. Spectral counts normalized to protein length[4] indicate that the KMN subcomplexes are the most abundant in the sample and the other core kinetochore proteins are present at relatively lower stoichiometry (Table S1), consistent with the silver-staining results (Fig. S2), and with fluorescence microscopy studies suggesting that the yeast KMN and Dam1 subcomplexes are most abundant on bi-oriented kinetochores[5]. Although the levels of Dam1 in our purifications are lower than KMN, kinetochores that are not attached to microtubules *in vivo* also have lower levels[6,7].

Note S2. Most of the CBF3 complex was not detected by mass spectrometry, consistent with the possibility that DNA may not co-purify with Dsn1-Flag.

Note S3. We concentrated the peak fraction (#44) after gel filtration and found that the pattern on a silver-stained SDS-PAGE gel was similar to the Flag eluate (data not shown), suggesting that the relative stoichiometry of core kinetochore proteins is similar before and after gel filtration.

Note S4. Our data provide strong evidence that the kinetochore particles must interact with the tips of the microtubules, because particle movement is driven by disassembling tips (Figs. 2 and 3) and because tension applied through the particles affects the dynamics of both growing and shortening tips (Fig. 4). However, the geometric arrangement of the kinetochore particles relative to the microtubule ends is uncertain. In principle, the particles could interact primarily with the 'outer' faces of the α/β tubulin dimers, which

are exposed in the lattice and also near the tip. Additionally, they could interact with structures that are found only at tips (i.e., exposed 'longitudinal', 'lateral', or 'lumenal' faces of the tubulin, or curved tubulin oligomers[8]). Also, the particles may or may not make 'end-on' attachments that resemble structurally those seen by electron microscopy in metazoans, where the kinetochores appear as a roughly planar fibrous meshwork and the microtubule tips are embedded nearly perpendicularly in the mesh[9].

Note S5. We found no evidence that the particles can track with growing tips in the absence of externally applied tension, i.e. 'autonomously'. However, we note that tip-attached kinetochores *in vivo* are usually under tension[10], and they are not known to track autonomously with growing tips. Instead, when the tension on a tip-attached kinetochore that is moving anti-poleward is suddenly lost (e.g., by laser ablation of its sister), the kinetochore ceases to move and adopts a 'neutral' or paused state[11]. This is similar to the behavior of the kinetochore particles: if a kinetochore-decorated bead is at first pulled so that it associates persistently with a growing microtubule end, and then the force is suddenly removed (by shuttering the laser trap), the bead ceases to move with the growing end. Likewise, fluorescent particles that appear initially to be bound at or near growing ends do not track with growth.

Note S6. Kinetochores in budding yeast are each thought to contain about six copies of Dsn1 (based on quantitative fluorescence measurements *in vivo*[5] and on the stoichiometry of proteins comprising the Mis12 subcomplex[1]). If the purified kinetochore particles also contain six Dsn1 molecules, then a Dsn1:bead ratio of 200:1 corresponds to a maximum

of ~33 particles per bead. Simple geometric considerations indicate that particles on only a small fraction of the bead surface, < 7 %, could simultaneously interact with a microtubule[12], indicating that coupling at low Dsn1:bead ratios was probably due to single kinetochore particles (see also, Fig. 3).

Note S7. The mean lifetime of attachment is equivalent to the mean first-passage time for detachment, $\langle t \rangle$, which can be expressed as a function of individual rate constants for any kinetic scheme with a finite number of states[13]. For the two-state catch bond-like model with the kinetochore initially bound to an assembling tip, the mean first-passage time is given by,

$$\langle t \rangle = \frac{k_1 + k_2 + k_4}{k_1 k_4 + k_2 k_3 + k_3 k_4},$$

where k_1, k_2, k_3, and k_4, represent the rates of catastrophe, rescue, detachment from assembly, and detachment from disassembly, respectively (the same rates displayed in Fig. 4b, 4c and 4d). The predicted lifetime curve in Fig. 4a was computed by substituting the best-fit exponential functions (Table S2) into the equation above.

3. Supplementary Tables

Table S1. Dsn1-Flag MS list (excel file link).

Table S2. Parameters for exponential curve fits shown in Fig. 4c and 4d. The force dependence of all four rates, k_1, k_2, k_3, k_4, was fit with the equation, $k_n(F) = k_n^o \exp\{F/F_n\}$, where F represents the applied force. The constants k_n^o and F_n represent the unloaded rate and the force required for an *e*-fold change, respectively.

n	**Transition**	**Unloaded rate** k_n^o (hr^{-1})	**Sensitivity** F_n (pN)
1	catastrophe	6.7 ± 2.0	-2.3 ± 0.5
2	rescue	86 ± 28	6.4 ± 4.2
3	detachment during assembly	0.4 ± 0.1	3.8 ± 0.8
4	detachment during disassembly	125 ± 61	-4.0 ± 3.1

Table S3. Yeast strains used in this study. All strains are isogenic with the W303 background.

Strain	Genotype	Used in Figure
SBY3	*MAT**a** ura3-1 leu2,3-112 his3-11 trp1-1 ade2-1 LYS2 can1-100 bar1Δ*	1a, b, S1, S2
SBY5640	*MAT**a** ura3-1::CSE4-3Flag::URA3 leu2,3-112 his3-11 trp1-1::256lacO:TRP1 ade2-1 LYS2 can1-100 cse4Δ::KAN PDS1-18myc::LEU2*	S1
SBY7441	*MAT**a** ura3-1 leu2,3-112 his3-11 trp1-1 ade2-1 lys2 can1-100 bar1Δ Dsn1-3Flag::KAN*	1a, b, c, S1, S2
SBY7464	*MAT**a** ura3-1 leu2,3-112 his3-11 trp1-1 ade2-1 lys2 can1-100 bar1Δ DSN1-3Flag::KAN NDC80-13myc::KAN*	S2
SBY7492	*MAT**a** ura3-1 leu2,3-112 his3-11 trp1-1 ade2-1 LYS2 can1-100 bar1Δ SPC105-3Flag::TRP1*	S1
SBY7870	*MAT**a** ura3-1 leu2,3-112 his3-11 trp1-1 ade2-1 LYS2 can1-100 bar1Δ NUF2-3Flag::KAN*	S1
SBY8193	*MAT**a** ura3-1 leu2,3-112 his3-11 trp1-1 ade2-1 lys2 can1-100 bar1Δ DSN1-3Flag::KAN NUF2-3GFP::HIS3*	S2, S7
SBY8253	*MAT**a** ura3-1 leu2,3-112 his3-11 trp1-1 ade2-1 can1-100 LYS2 bar1Δ DSN1-6His-3Flag::URA3*	1d, 2a, 3, 4, S1, S2, S3, S4, S8, S9, S10
SBY8332	*MAT**a** ura3-1 leu2,3-112 his3-11 trp1-1 ade2-1 can1-100 LYS2 bar1Δ DSN1-6His-3Flag::URA3 NUF2-3GFP::HIS3 MTW1-mCherry::HPH*	S2
SBY8334	*MAT**a** ura3-1 leu2,3-112 his3-11 trp1-1 ade2-1 can1-100 LYS2 bar1Δ DSN1-6His-3Flag::URA3 NUF2-3GFP::HIS3 MIF2-mCherry::HPH*	S2
SBY8362	*MAT**a** ura3-1 leu2,3-112 his3-11 trp1-1 ade2-1 can1-100 LYS2 bar1Δ DSN1-6His-3Flag::URA3 ndc80-1*	2a, 3, S4
SBY8381	*MAT**a** ura3-1 leu2,3-112 his3-11 trp1-1 ade2-1 can1-100 LYS2*	2a, 3, S4

	bar1Δ DSN1-6His-3Flag::URA3 spc105-15	
SBY8460	*MAT**a** ura3-1 leu2,3-112 his3-11 trp1-1::256lacO::TRP1 ade2-1 can1-100 LYS2 bar1Δ DSN1-6His-3Flag:URA3 dad1-1::KAN*	2a, 3
SBY8505	*MAT**a** ura3-1 leu2,3-112 his3-11 trp1-1 ade2-1 can1-100 LYS2 bar1Δ DSN1-6is-3Flag::URA3 YDR532c-GFP::HIS3*	S2
SBY8506	*MAT**a** ura3-1 leu2,3-112 his3-11 trp1-1 ade2-1 can1-100 LYS2 bar1Δ DSN1-6His-3Flag::URA3 SPC105-GFP::HIS3*	S2
SBY8564	*MAT**a** ura3-1 leu2,3-112 his3-11 trp1-1 ade2-1 LYS2 can1-100 bar1Δ MTW1-3Flag::KAN*	S1
SBY8584	*MAT**a** ura3-1::CSE4-GFP::URA3 leu2,3-112 his3-11 trp1-1 ade2-1 can1-100 lys2 bar1Δ DSN1-6His-3Flag::URA3 cse4Δ::KAN*	S2
SBY8678	*MAT**a** ura3-1::CSE4-GFP::URA3 leu2,3-112 his3-11 trp1-1 ade2-1 can1-100 lys2 bar1Δ DSN1-6His-3Flag::URA3 cse4Δ::KAN MTW1-mCherry::HPH ndc80-1*	2c, S5, S6
SBY8680	*MAT**a** ura3-1::CSE4-GFP::URA3 leu2,3-112 his3-11 trp1-1 ade2-1 can1-100 lys2 bar1Δ DSN1-6His-3Flag::URA3 cse4Δ::KAN MTW1-mCherry::HPH*	2c, 2d, S5, S6

Table S4. Plasmids used in this study.

Plasmid	Description
pBS35	*mCherry, HPH* (gift from Yeast Resource Center (mCherry from Roger Tsien)
pGEX-2T	*GST expression vector*
pSB167	*12Myc, URA3* (integrating)
pSB450	*pFA6a-TRP1*
pSB623	*3GFP, HIS3* (gift from David Pellman, PB1585)
pSB624	*DSN1, CEN, URA3*
pSB812	*3Flag, KAN* (gift from Toshi Tsukiyama, p3Flag-KANMX)
pSB897	*NUF2-3GFP, HIS3* (integrating)
pSB1110	*DSN1-12Myc, URA3* (integrating)
pSB1113	*DSN1-3Flag, URA3* (integrating)
pSB1265	*3Flag, TRP1*
pSB1590	*DSN1-6His-3Flag, URA3* (integrating)
pSB1617	*CSE4-GFP, URA3* (integrating)
pSB1643	*GST-SPC105 (1-798 bp) expression vector*

4. Supplementary Movie legends

Movie S1. Cse4-GFP kinetochore particles track with depolymerizing microtubule tips.

Dynamic microtubules were polymerized from Alexa 647 tubulin in the presence of Cse4-GFP kinetochore particles (at 10 nM Dsn1-Flag). Depolymerization was triggered by removing the free tubulin via buffer exchange, causing a significant decrease in red background fluorescence and subsequent disassembly-driven movement of microtubule-bound kinetochore particles (arrows indicate the filament shown in Fig. 2d). The movie was recorded at 10 frames s^{-1} and is displayed here at ×10 speed. Scale bar, 3 μm.

Movie S2. Nuf2-3GFP kinetochore particles track with shortening tips.

This movie (corresponding to the microtubule shown in Fig. S7) was collected using the same protocol as Movie S1, with the exception that kinetochore particles were labeled via Nuf2-3GFP. It was recorded at 10 frames s^{-1} and is displayed here at ×4 speed. Scale bar, 2 μm.

Movie S3. Purified kinetochore particles couple force to dynamic microtubules.

Movement of an end-associated bead is coupled to multiple rounds of microtubule assembly and disassembly under 1.7 pN of constant tension, applied by a laser trapping-based force clamp. The end-associated bead is held in a fixed position in the laser trap while the stage is moved under feedback control to accommodate changes in microtubule length. A second bead, stuck to the coverslip, serves as a fiducial illustrating the stage movement. Leftward movement corresponds to filament growth and rightward

movement corresponds to shortening. Beads were prepared with kinetochore material at a Dsn1:bead ratio of 200:1. The movie was recorded at 30 frames s^{-1} using differential interference contrast microscopy and is shown here at ×60 speed.

5. Supplementary References

1. De Wulf, P., McAinsh, A. D. & Sorger, P. K. Hierarchical assembly of the budding yeast kinetochore from multiple subcomplexes. *Genes Dev* **17**, 2902-2921 (2003).

2. Wei, R. R., Sorger, P. K. & Harrison, S. C. Molecular organization of the Ndc80 complex, an essential kinetochore component. *Proc Natl Acad Sci U S A* **102**, 5363-5367 (2005).

3. Tien, J. F. *et al.* Cooperation of the Dam1 and Ndc80 kinetochore complexes enhances microtubule coupling and is regulated by aurora B. *J Cell Biol* **189**, 713-723 (2010).

4. Liu, H., Sadygov, R. G. & Yates, J. R., 3rd. A model for random sampling and estimation of relative protein abundance in shotgun proteomics. *Anal Chem* **76**, 4193-4201 (2004).

5. Joglekar, A. P., Bouck, D. C., Molk, J. N., Bloom, K. S. & Salmon, E. D. Molecular architecture of a kinetochore-microtubule attachment site. *Nat Cell Biol* **8**, 581-585 (2006).

6. Li, Y. *et al.* The mitotic spindle is required for loading of the DASH complex onto the kinetochore. *Genes Dev* **16**, 183-197. (2002).

7. Enquist-Newman, M. *et al.* Dad1p, third component of the Duo1p/Dam1p complex involved in kinetochore function and mitotic spindle integrity. *Mol Biol Cell* **12**, 2601-2613. (2001).

8. McIntosh, J. R. *et al.* Fibrils connect microtubule tips with kinetochores: a mechanism to couple tubulin dynamics to chromosome motion. *Cell* **135**, 322-333 (2008).

9. McEwen, B. F. & Dong, Y. Contrasting models for kinetochore microtubule attachment in mammalian cells. *Cell Mol Life Sci* **67**, 2163-2172 (2010).

10. Waters, J. C., Skibbens, R. V. & Salmon, E. D. Oscillating mitotic newt lung cell kinetochores are, on average, under tension and rarely push. *J Cell Sci* **109**, 2823-2831 (1996).

11. Khodjakov, A. & Rieder, C. L. Kinetochores moving away from their associated pole do not exert a significant pushing force on the chromosome. *J Cell Biol* **135**, 315-327 (1996).

12. Powers, A. F. *et al.* The Ndc80 kinetochore complex forms load-bearing attachments to dynamic microtubule tips via biased diffusion. *Cell* **136**, 865-875 (2009).

13. Shaevitz, J. W., Block, S. M. & Schnitzer, M. J. Statistical kinetics of macromolecular dynamics. *Biophys J* **89**, 2277-2285 (2005).